Published in final edited form as:
Am J Physiol. 1999 September ; 277(3 Pt 2): H1241–H1251.

Cardiac endothelial transport and metabolism of adenosine and inosine

Lisa M. Schwartz, **Thomas R. Bukowski**, **James H. Revkin**, and **James B. Bassingthwaighte**
Department of Bioengineering, University of Washington, Seattle, Washington 98195-7962

Abstract

The influence of transmembrane flux limitations on cellular metabolism of purine nucleosides was assessed in whole organ studies. Transcapillary transport of the purine nucleosides adenosine (Ado) and inosine (Ino) via paracellular diffusion through interendothelial clefts in parallel with carrier-mediated transendothelial fluxes was studied in isolated, Krebs-Henseleit-perfused rabbit and guinea pig hearts. After injection into coronary inflow, multiple-indicator dilution curves were obtained from coronary outflow for 90 s for ^{131}I-labeled albumin (intravascular reference tracer), [^{3}H]arabinofuranosyl hypoxanthine (AraH; extracellular reference tracer and nonreactive adenosine analog), and either [^{14}C]Ado or [^{14}C]Ino. Ado or Ino was separated from their degradative products, hypoxanthine, xanthine, and uric acid, in each outflow sample by HPLC and radioisotope counting. Ado and Ino, but not AraH, permeate the luminal membrane of endothelial cells via a saturable transporter with permeability-surface area product PS_{ecl} and also diffuse passively through interendothelial clefts with the same conductance (PS_g) as AraH. These parallel conductances were estimated via fitting with an axially distributed, multi-pathway, four-region blood-tissue exchange model. PS_g for AraH were ~4 and 2.5 ml · g^{-1} · min^{-1} in rabbits and guinea pigs, respectively. In contrast, transplasmalemmal conductances (endothelial PS_{ecl}) were ~0.2 ml · g^{-1} · min^{-1} for both Ado and Ino in rabbit hearts but ~2 ml · g^{-1} · min^{-1} in guinea pig hearts, an order of magnitude different. Purine nucleoside metabolism also differs between guinea pig and rabbit cardiac endothelium. In guinea pig heart, 50% of the tracer Ado bolus was retained, 35% was washed out as Ado, and 15% was lost as effluent metabolites; 25% of Ino was retained, 50% washed out, and 25% was lost as metabolites. In rabbit heart, 45% of Ado was retained and 5% lost as metabolites, and 7% of Ino was retained and 3% lost as metabolites. We conclude that endothelial transport of Ado and Ino is a prime determinant of their metabolic fates: where transport rates are high, metabolic transformation is high.

Keywords

nucleoside transport; species specificity; biological transport; multiple-indicator dilution technique; capillary endothelial permeability; blood-tissue exchange; isolated heart; rabbit; guinea pig

Address for reprint requests and other correspondence: J. B. Bassingthwaighte, Univ. of Washington, Dept. of Bioengineering, Box 357962, Seattle, WA 98195-7962 (jbb@nsr.bioeng.washington.edu).

Present addresses: L. M. Schwartz, Physiology Dept., Uniformed Services Univ. of the Health Sciences, 4301 Jones Bridge Rd., Bethesda, MD 20814-4799; T. R. Bukowski, Zymogenetics, 1201 Eastlake Ave. East, Seattle, WA 98102-3702; J. H. Revkin, Yale Univ. School of Medicine, Fitkin 3 (3FMP), New Haven, CT 96510.

The authors appreciate the help of Joseph I. S. Chan and Gary M. Raymond in the development of the model-fitting program (SENSOP) and thank them and Dr. Zheng Li for the model programs, MMID4 and GENTEX. These are available by downloading the simulation system, XSIM, at http://nsr.bioeng.washington.edu. The assistance of James Ploger in experimentation and analysis and the expertise of Eric Lawson in the manuscript and figure preparation are deeply appreciated.

Adenosine (Ado) is important as a potential regulator of vasomotion in the heart, especially during conditions of hypoxia or increased metabolic rate (9,22,47) and also appears to have a cardioprotective role during myocardial ischemia (21,23). Endothelial cells play a major role in the regulation of the vasoactive interstitial pool of Ado and the salvage of nucleoside lost from the myocyte, functioning as both a physical and a metabolic barrier between the vascular and interstitial space (35,48). Endothelial cells appear to dominate the uptake of infused Ado (26,40) and exhibit a high rate of metabolism, converting vascularly infused Ado to ino-sine (Ino), hypoxanthine (Hx), xanthine (Xa), uric acid (UA), and phosphorylated compounds (1,8,24,26). Quantitative measures of nucleoside transport and metabolism by endothelial cells are critical to understanding the regulation of interstitial Ado concentrations and nucleoside salvage (35,48).

Cultured aortic and pulmonary endothelial cells exhibit carrier-mediated plasma membrane transport of Ado (17,43). Indicator dilution studies of intact perfused lung (14,29) and skeletal muscle (26) demonstrated that uptake of Ado is carrier mediated in in situ endothelial cells and is blocked by dipyridamole. Because Moffett et al. (38) found that endothelial serotonin uptake was high in rabbit lungs but zero in the heart, we know that measures of transport and metabolism must be made explicitly in the setting for which the values are needed and cannot be taken from another organ or species.

Wangler et al. (51) demonstrated that capillary endothelial cells of guinea pig hearts avidly take up and metabolize [^{3}H]Ado. Mohrman and Heller (39) reported, after conducting steady-state, nontracer experiments in guinea pig and rat heart, that these two species differed in the degree to which Ino competitively reduced Ado uptake and retention. Although it is often assumed in tissue and isolated organ studies that substrate metabolism is occurring in the parenchymal cells of the organ, in reality it may be the endothelial Ado transport mechanisms that explain numerous species differences reported in the metabolism on the physiological effects of Ado and its metabolites (30,52). Because endothelial cells normally lie between the blood, on which the observations of effluent concentrations are made, and the cardiomyocytes, it is important to characterize endothelial events accurately.

The capillary endothelium provides two possible parallel paths for purine nucleoside to travel between blood and myocytes, the paracellular or interendothelial cleft pathway for passive diffusion and the transcellular route crossing both luminal and abluminal surfaces of the endothelial cell by a carrier-mediated, saturable transporter. Studies in isolated cells, myocytes, or endothelial cells cannot predict the balance of fluxes occurring in vivo.

The present studies are designed to examine the conductances for Ino and Ado by the nucleoside transporter of cardiac capillary endothelial cells in the intact heart functioning in perfuso, using high-resolution multiple-indicator dilution (MID) tracer studies to obtain estimates of the permeability-surface area products (*PS*) for the clefts separately from those for the transporters. A further goal is to define the differences in nucleoside transport between guinea pigs and rabbits, both of which are used in studies of cardiac ischemia, reperfusion, or energy balance. The MID methodology is suited for eliciting information on fast reaction rates or transfer rates when used in conjunction with modeling analysis for blood-tissue exchange processes (5,6). It is the method giving the highest resolution for endothelial studies.

The results show that although the overall capillary conductances for purine nucleosides are similar in rabbit and guinea pig, the endothelial carrier-mediated component is an order of magnitude higher in guinea pigs than in rabbits. This difference has a major impact on the interpretation of physiological responses to the release of Ado from myocytes during

hypoxia or ischemia and on the estimated interstitial concentrations reaching receptors on smooth muscle cells.

Glossary

F_p	Flow of solute-containing perfusate, ml · g^{-1} · min^{-1}
PS_g	Permeability-surface area product for passive transport through gaps between endothelial cells, ml · g^{-1} · min^{-1}
PS_{ecl}	Permeability-surface area product for endothelial luminal or plasma surface, ml · g^{-1} · min^{-1}
PS_{eca}	Abluminal endothelial permeability-surface area product, ml · g^{-1} · min^{-1} (assumed = PS_{ecl})
PS_{pc}	Permeability-surface area product for parenchymal cells (myocytes), ml · g^{-1} · min^{-1}
G_{ec}	First-order clearance by consumption or gulosity in the endothelial cell, without return of the reactant (Ado: sum of rate constant for deamination reactions + Ado kinase reaction; Ino: rate constant for conversion to Hx via purine nucleoside phosphorylase) ml · g^{-1} · min^{-1}. Metabolic flux = G_{ec} × intraendothelial concentration.
G_{pc}	First-order clearance by consumption or gulosity in the parenchymal cell, without return, ml · g^{-1} · min^{-1}
V_p	Intracapillary volume, ml/g
V'_{ec}	Virtual endothelial cell volume of distribution, ml/g
V'_{isf}	Virtual interstitial fluid volume of distribution, ml/g
V'_{pc}	Virtual parenchymal cell volume of distribution, ml/g

METHODS

Animal preparation

Adult guinea pigs (250–550 g) and New Zealand White rabbits (3–4 kg) were heparinized and anesthetized with pentobarbital sodium (guinea pigs: 50 mg/kg ip; rabbits: 40 mg/kg iv). Their hearts were rapidly excised and immersed in ice-cold modified Krebs-Ringer bicarbonate buffer (KRB; in mM: 118 NaCl, 3.8 KCl, 1.2 KH_2PO_4, 2.1 $CaCl_2H_2O$, 0.70 $MgSO_4 \cdot 7H_2O$, 0.1 EDTA, 11.0 glucose, and 25 $NaHCO_3$ with 0.1% bovine serum albumin). The aorta was cannulated, and the coronary arteries were perfused with KRB, Langendorff style. The perfusate was preequilibrated with 95% O_2-5% CO_2 and maintained at 37°C and pH 7.4 and was not recirculated. A side-hole catheter was inserted though the apex of the right ventricle (RV) and secured in the pulmonary artery at a point ~2 in. above the base of the heart for outflow collection from the coronary sinus, right atrium, and RV. The cannula volume was ~0.1 ml, and the RV cavity was continuously emptied by the suction caused by the weight of fluid in the cannula so that there was minimal delay to efflux. The left ventricle was vented via a no. 22 needle through the thinnest point of the apical myocardium to prevent ventricular filling by leakage through the aortic valve or thebesian drainage. The perfusion rate was controlled with a roller pump on the inflow line, and perfusion pressure and heart rate were measured with a transducer on the arterial cannula. Hearts were electrically paced (guinea pigs: 300 beats/min; rabbits: 180 beats/min). The preparation was allowed to stabilize for 20 min before the experiment began to wash out all red blood cells and to allow the heart weight to reach steady state.

Experimental protocol

The single-pass MID technique was used to quantify the capillary extraction of Ino and Ado. ^{131}I-labeled albumin (mol wt = 68,000) was synthesized as described below and used as the intravascular reference tracer to assess the delay in the arterial, capillary, and venous vascular beds. To make ^{131}I-albumin, bovine serum albumin (Sigma) was radioiodinated

using chloramine T (Sigma) and sodium thiosulfate (Sigma) as described previously (37). The reaction mixture was immediately chromatographed on a 3.9-mm × 30-cm Sephadex G-25 column equilibrated with NaH_2PO_4 (pH 7.5), and fractions corresponding to peak activity were collected. One milliliter of the collected effluent was dialyzed overnight at 4°C (Spectrophor tubing) against one liter of KRB and vacuum filtered (0.2 μm) to remove free ^{131}I and any macroscopic albumin impurities.

Use of an analog of Ado that is restricted to the extracellular region, 9-β-D-arabinofuranosyl hypoxanthine (AraH, mol wt = 267), allowed evaluation of the additional process of permeation of the capillary wall via extracellular pathways and distribution in interstitial fluid (ISF) volume. One millicurie of [U-^{3}H]arabinofuranosyl adenine (10–20 Ci/mmol; ICN) was evaporated to dryness and resuspended in one milliliter of phosphate buffer (50 mM; pH 7.5). Deamination was achieved by adding 120 units of Ado deaminase (Sigma type III) and incubating at room temperature for 0.5 h. The deaminase was inactivated with the addition of perchloric acid, and the solution was neutralized with KOH. The AraH fraction was then isolated using HPLC. This fraction was evaporated to dryness at 45°C on a vortex evaporator, stored at −20°C, and resuspended in KRB on the day of the experiment. Lack of residual enzyme activity was verified spectrophotometrically.

Aliquots of [U-^{14}C]Ino (378 mCi/mmol, mol wt = 268; Amersham) and [U-^{14}C]Ado (515 mCi/mmol, mol wt = 269; Amersham) were purified on HPLC <72 h before experimental use, dried, frozen, and redissolved in KRB on the day of the experiment. Contaminants in the form of UA, Xa, Hx (and for Ado injections, Ino) constituted <2% of total in the injected dose, and these can be detected in the first few samples of the outflow-dilution curves.

Indicator dilution curves were obtained by injecting a bolus [rabbits: 0.4 ml containing (in μCi) ~4 albumin, 2.5 AraH, and 2.5 Ado or Ino; guinea pigs: 0.1 ml containing (in μCi) ~1 albumin, 0.7 AraH, and 0.7 Ado or Ino] into the aortic root. Immediately before this injection, collection of outflow samples from the RV into 60 cold, tared test tubes was begun. The sampling interval was 1 s for *tubes 1–30* and 2 s for *tubes 31–60*. Tubes contained 250 (*samples 1–30*) or 500 (*samples 31–60*) μl of "stop solution" composed of 32 μM dipyridamole (Persantin, gift from Boehringer Ingelheim) and 3 μM erythro-9-(2-hydroxy-3-nonyl)adenine HCl (Burroughs Wellcome) to prevent the cellular uptake and deamination of Ado, particularly by any red blood cells that might have remained in the heart and washed out into the collection tubes. Control experiments verified that this solution prevented degradation of Ado in collected effluent.

Ado and Ino indicator dilution curves were obtained in each heart, allowing 10 min between injections to enable complete washout of labeled tracers from the heart. Additionally, in two rabbit and two guinea pig hearts, bolus injections containing radiolabeled ^{131}I-albumin, [^{14}C]sucrose (NEC 100× uniformly labeled, 500 mCi/mmol, mol wt = 344), and [^{3}H]AraH were made to test the validity of AraH as an extracellular, interstitial marker.

Sample processing

Outflow samples were shaken immediately after collection to mix the solution and effluent. Each sample was then weighed, and a 100-μl aliquot was removed and placed in a labeled counting tube for 10-min ^{131}I counting in a gamma counter. Samples were kept ice cold throughout processing. The remainder of the sample was frozen for separation of nucleosides using HPLC techniques. Because samples contained metabolites, we could not simply use the triple-label counting technique described previously (11), but that study gives the details of our liquid scintillation counting methods. Duplicates of three dilutions of each injected dose were made in collected effluent and processed identically.

One hundred-microliter aliquots of collected samples and doses were assayed on a Waters HPLC system using a 25-min isocratic method and C-18 stainless steel column (125-Å pore size, 30 cm × 3.9 mm; μBondapak, Waters) at a flow rate of 1 ml/min (28). The mobile phase consisted of 10 mM $NH_4H_2PO_4$ (pH 5.5) and 100% methanol (10:1 vol/vol). The eluted fractions corresponding to Ado, Ino + AraH (coeluted), Hx, Xa, and UA were collected and added to scintillation cocktail Redisolv MP (11) for 10-min beta counting (LS-5800, Beckman Instruments). Corrections were made for efficiency and, for the Ino + AraH fraction, the overlap of ^3H and ^{14}C in the energy spectra of their emissions. Tracer recoveries using these methods were 95–99.5%.

Data analysis

Each dilution curve was normalized with respect to injected activity and expressed as the fraction of injected tracer emerging per second, $h(t)$ (36). The area of the outflow dilution curve and the mean transit time through the heart for each tracer were calculated from each of the normalized $h(t)$ curves. Extractions of AraH, Ado, and Ino were calculated using the formula $E(t) = 1 - h_D(t)/h_R(t)$, where $E(t)$ is the instantaneous extraction at *time t,* $h_D(t)$ is the fraction of permeating tracer exiting per unit time, and $h_R(t)$ is that for the intravascular reference tracer. The values of $E(t)$ were used to give a rough estimate of the capillary *PS* (PS_C) for the diffusible tracers using the Crone-Renkin equation

$$PS_c = -F_p \log_e(1 - E_{max}) \quad (1)$$

where E_{max} is the maximal instantaneous extraction, estimated by smoothing through the peak of the curve of $E(t)$. When there is no return flux from tissue to capillary perfusate, PS_C represents the sum of $PS_g + PS_{ecl}$, that is, the sum of *PS* for the luminal surface of endothelial cells plus that of the gaps between adjacent endothelial cells.

The indicator dilution curves underwent more precise analysis with a four-region, three-barrier mathematical model of tracer transport that is described in detail elsewhere (6,26,51) and augmented to account for transient interstitial binding of AraH. Bassingthwaighte et al. (2) described the numerical methods. Parameters used in fitting the data are shown in the schematic representation of the capillary unit (Fig. 1) and are defined in the *Glossary*.

For albumin, the model was described solely by $h_R(t)$ and the transport through the set of parallel capillary tissue units without any exchange with the extravascular regions. The total flows are measured and the heterogeneity taken as known from similar experiments in which microsphere distributions were measured. Intravascular volume (V_p) was estimated from vascular casting techniques to be ~0.07 ml/g in the heart (an approximation for capillary density of ~3,000/ mm^2 with average diameters of 5.6 μm, e.g., from Ref. 7). Wangler et al. (51) showed that substantial variation in the value taken for V_p has little influence on the estimates of the other parameters, so V_p was assumed to be constant: we used $V_p = 0.06$ ml/g instead of 0.07 ml/g to compensate for the low perfusion pressures in the preparation. The outflow albumin curve was deconvoluted via the intravascular model to define the input concentration-time curves for all of the simultaneously injected tracers.

The other volumes were given fixed values in accord with the total water space of 0.83 ml/g: $V'_{ec}=0.02$, $V'_{isf}=0.35$, and $V'_{pc}=0.40$ ml/g, smaller than in vivo (25), because of interstitial swelling.

On the assumption that the regional flow heterogeneity was well approximated by a 20-pathway truncated Gaussian distribution with a relative dispersion between 50 and 60%, the albumin fit was used to define the input concentration-time curves of simultaneously injected tracers by deconvolution. This approach has been described in the methods of

Kuikka et al. (36), is based on the principles detailed by Bassingthwaighte and Goresky (3), and makes use of the data on regional flows using the tracer microsphere technique (4).

The second phase of the modeling strategy was to fit the indicator dilution curve for the extracellular reference, AraH, with a two-region capillary-ISF model, allowing permeation only through the interendothelial cellular clefts and giving estimates of PS_g. The values for V'_{isf} in these KRB-perfused hearts are larger than those for the blood-perfused hearts of Gonzalez and Bassingthwaighte (25), which averaged 0.18 ml/g. Extremely large values were found for sucrose space by Vargas and Johnson (49,50), up to 0.45 ml/g in rabbit hearts perfused without albumin in the perfusate. Because accuracy of the estimates of V'_{isf} from AraH was compromised by the complication of interstitial binding of AraH and because the sensitivity of transmembrane transport parameters of Ino and Ado is almost unaffected by even 20% error in estimates of V'_{isf} (6), we used the value of 0.35 ml/g without adjustment in the analysis. The AraH outflow curves required accounting for additional delay and dispersion, which was accomplished by allowing for binding to an extracellular interstitial site as described in the APPENDIX. This required two additional parameters to be adjusted in the optimization to fit the AraH curves: one is B_T/K_d, the ratio of a binding site concentration to the dissociation constant for its binding with AraH. The other is k_1, the rate of association of AraH with the site, as seen in Eqs. A1 and A2. The k_1 would not be needed if the association were rapid, as for near-equilibrium binding.

Finally, Ado and Ino dilution curves were fitted: the values for PS_g(Ado) or PS_g(Ino) were taken to be those for PS_g(AraH) because the molecular weights are similar and the expected relative diffusion coefficients and permeabilities through the interendothelial clefts should be the same. Because of the high rates of intraendothelial uptake or conversion of Ado and Ino, values for the conductance across the abluminal surface of the endothelial cell (PS_{eca}) were impossible to determine accurately within the range from 1 to 10 times those of the luminal surface (PS_{ecl}); consequently, we fixed $PS_{eca} = PS_{ecl}$. The optimization routine matching the model solutions to the observed dilution curves therefore adjusted only PS_{ecl}, PS_{pc}, and the values for the first-order consumption or gulosity (G_{ec} and G_{pc}). Of these, PS_{ecl} is well determined and G_{ec} only slightly less so (2,6), whereas PS_{pc} and G_{pc} are estimated with less accuracy.

The optimization routine, SENSOP (15), running under the simulation interface XSIM, is an improved Levenberg-Marquardt steepest-descent method that provides confidence estimates on the values of the estimated parameters. The model programs, MMID4 from Bassingthwaighte et al. (6) and GENTEX from Dr. Zheng Li, can be downloaded from the National Simulation Resource website at http://nsr.bioeng.washington.edu, along with XSIM. MMID4 is model #305, Gentex is #84 and both can be run over the web under the simulation system JSim at www.physiome.org, or downloaded and run on one's own computer.

RESULTS

Hemodynamic data

Mean perfusion pressure at the time of injection was 42 ± 1 mmHg in rabbits and 35 ± 2 mmHg in guinea pigs. Perfusate flow averaged 4.5 ± 0.2 ml · g^{-1} · min^{-1} for rabbits and 5.0 ± 0.4 ml · g^{-1} min^{-1} for guinea pigs. These flows are suitable for providing oxygenation for these beating hearts that do no external work, and the perfusion pressures are low enough to minimize cardiac edema.

Validation of AraH as an extracellular marker for estimating PS_g

Four sets of indicator dilution curves were obtained after bolus injections of tracer albumin, sucrose, and AraH, two in each species. Albumin, AraH, and sucrose recoveries were >98% in both species, indicating that no metabolism of these substances occurred during the measurement period. The relative PS_g for AraH and sucrose can be estimated from the ratio of their free diffusion coefficients (D). Calculating these from the square root of the reciprocals of the ratio of their molecular weights gives the ratio D(Ado)/ D(Suc) at 1.12, but this is not an accurate method. A better method is to estimate from the molecular shapes and volumes [following Ref. 20, which gives D(Ado)/ D(Sucrose) = 1.2]. This should be appropriate given that AraH does not enter cells. AraH is not taken up by erythrocytes in either the presence or the absence of dipyridamole (26) and therefore does not use the purine transporter or block the transporter (41). However, the model analysis of outflow curves indicated that AraH has a high extravascular volume of distribution, as if it attaches to surface sites in the interstitium. Values of this additional binding space, $V'_{isf} \cdot B_T/K_d$, were found to be 0.70 ± 0.3 ml/g (n = 16). Values of the association rate (k_1) were found to average ~0.3 ± 0.4 $M^{-1} \cdot s^{-1}$ (n = 16); these rates are too slow to allow the simplification to assume equilibrium binding. Because they are slow, there is some influence on the model solutions; therefore, accounting for the slow exchange with the binding site did improve their fits to the data.

Use of this accounting for the enlarged V'_{isf}(AraH) in the model analysis gave estimates of PS_g for AraH of 1.2 ± 0.05 (n = 4) times those for sucrose. (These data support the use of AraH as a reference marker because it accounts appropriately for permeation through clefts, but accounting for the binding is a technical nuisance and reduces the efficiency of analysis of the Ino and Ado data, so we have decided to use sucrose as the reference solute for future experiments.) For analyzing these experiments, we have assumed that values of PS_g for Ino and Ado are identical to those for the AraH injected simultaneously.

Outflow dilution data for Ino and Ado

There were 16 sets of MID curves, 8 in rabbit hearts and 8 in guinea pig hearts. Table 1 lists for these the flows and extraction maxima (E_{max}) of the smoothed curves for the instantaneous extraction, $E(t) = 1 - h(t)/h_R(t)$, where $h(t)$ is the normalized effluent dilution curve for the test substance and $h_R(t)$ is that for the intravascular reference albumin. E_{max} is a function of solute escape through both pathways, interendothelial cleft plus endothelial transporter.

As a secondary feature of these studies, we have estimated the capillary PS by the Crone-Renkin expression $PS_c = -F \log_e (1 - E_{max})$ and by the full model. AraH had an average E_{max} of 50 ± 5% for all eight rabbit studies (Table 1). For eight rabbits, PS_c(AraH) averaged 3.08 ± 0.58 ml $\cdot$ g^{-1} $\cdot$ min^{-1}. However, this calculation does not account for reflux from the ISF to the capillary and therefore underestimates PS_g. With the full model, PS_g(AraH) averaged 3.92 ± 0.88 ml $\cdot$ g^{-1} $\cdot$ min^{-1}, that is, PS_c underestimated PS_g by a little over 20%, even at these fairly high flows. In the eight guinea pig hearts, the peak extractions of AraH were 38 ± 4% and PS_c(AraH) averaged 2.39 ± 0.51 ml $\cdot$ g^{-1} $\cdot$ min^{-1}, again lower than that obtained by using the full model, PS_g = 2.58 ± 0.59 ml $\cdot$ g^{-1} $\cdot$ min^{-1}.

The percent recoveries of untransformed purine nucleoside tracer are also listed in Table 1. In the rabbit, 89% of the injected Ino is recovered as Ino in the effluent but only 53% of the Ado is recovered unchanged. In the guinea pig, the tracer recoveries are only 51% for Ino and 41% for Ado. Although E_{max} are not greatly different between the two species, values of E_{max} are governed not only by the sum of PS_g (cleft) + PS_{ecl} (transporter) but also by back-diffusion of either un-transformed or transformed tracer from ISF to capillary. Another

potential influence is flow heterogeneity (34). Note that E_{max} for Ado and Ino are little greater than those for AraH in rabbits but much greater in guinea pigs, in which the percent tracer recoveries in the effluent are much lower. Modeling analysis is critical to analyze the data from both species adequately.

The outflow dilution quantitation required HPLC separation of metabolites in each sample so that the time course of metabolite appearance in the effluent and the fractional transformation over the 1.5 min of data acquisition can be calculated. The fractions of the injected Ino or Ado metabolized to each degradation product are shown in Table 2 for the studies in which we acquired the data. In the rabbit, a little Ino is transformed to Hx, but the recoveries of Xa and UA were indistinguishable from contamination by oxidation of the injectate, as is expected in the absence of xanthine oxidase. For Ado in the rabbit, 3–5% appears as Ino but almost one-half is still retained at the end of 90 s, presumably because other intracellular reactions for Ado (e.g., AMP formation via Ado kinase) are more likely to use Ado than is deamination to produce Ino.

In the guinea pig, the degradation through the pathway is much more important, because 20% of the Ino and 10% of the Ado appears as UA. Additionally, much more Ino is retained in the guinea pig (27%) compared with 7% in the rabbit. This may reflect activity of the Hx salvage pathway. As for Ado, the retention is higher yet (~50%), and because so little Ino or UA is produced, most of this is probably phosphorylated by Ado kinase returned as nucleotide, presumably ATP.

Ino outflow dilution data: rabbit

The normalized outflow dilution curve for one experiment in a rabbit heart is shown in Fig. 2. Albumin, the unextracted intravascular reference tracer, has a relatively high, narrow peak and rapid decline relative to the permeating solutes. AraH, the extracellular marker, diffuses into the ISF via the clefts between the endothelial cells. The escape of AraH from the plasma space is reflected in the decreased peak height of the AraH outflow curve relative to albumin and in the subsequent later crossover of the two curves. These phenomena are common to solutes that have a total volume of distribution larger than V_p and which are not consumed. Ino is extracted only slightly more than AraH, as evidenced by the Ino curve being almost superimposable on the AraH curve. The minimal back-diffusion of Ino from the extravascular space and the failure to cross over above the AraH curve after the peak indicates that much of the Ino that entered the cells was either metabolized or retained. However, metabolism of injected Ino was very low in rabbit hearts and recovery of tracer Ino was 89 ± 2% (SD, $n = 4$). An additional 3 ± 1% of the tracer was recovered as Hx; the levels of Xa and UA were not distinguishable from zero.

Peak extraction of Ino (E_{max}), occurring during the early upslope and peak phase of the curve, averaged 53 ± 4% in rabbit hearts. Corresponding estimates of total capillary PS_C(Ino) from the Crone-Renkin equation averaged 3.38 ± 0.56, little different from values for AraH, implying that the transporter protein is scarce on the rabbit endothelial luminal surface (see Table 1). Accordingly, using the full model [where PS_g(Ino) = PS_g(AraH) by assumption], the values of PS_{ecl}(Ino) averaged 0.1 ± 0.2 ml · g^{-1} · min^{-1} (see Table 3).

Ino outflow dilution data: guinea pigs

The normalized outflow dilution curves for one experiment in a guinea pig are shown in the lower panel of Fig. 2. Although these are qualitatively similar to the corresponding set of dilution curves in the rabbit, quantitative differences in Ino uptake and metabolism are evident. The lower peak height for tracer Ino relative to AraH indicates its greater rate of permeation of the endothelial surface in the guinea pig hearts. Ino had an average E_{max} of 53

± 1%. The calculated PS_C(Ino) averaged 3.70 ± 0.82, and, being larger than that for AraH, showed substantial endothelial cell uptake of Ino in guinea pig hearts.

Ino was rapidly metabolized in the guinea pig heart; recovery of injected tracer Ino averaged 50 ± 3% ($n = 4$). Analysis of metabolic products appearing in the outflow samples indicated that UA constituted the major metabolic product measured (18–23% of injected tracer). Hx and Xa each made up ≤2% of the product of injected tracer.

Ado outflow dilution data: rabbits

The normalized outflow dilution curve for one rabbit experiment is shown in Fig. 3, *left*. Although relatively small differences in peak height are evident between AraH and Ado, there are large differences between the two tracers in the tails of the curves. Although the ratio of PS_C for Ado relative to AraH (1.09) indicates that little Ado is transported across the luminal surface of rabbit endothelial cells, recovery of Ado was only 50%. About 40% of the injected tracer Ado appeared in the outflow, 3% as Ino and 1% as Hx. Neither Xa nor UA was recovered from the outflow in rabbit experiments, the data after the first 10 s not being different from methodological noise; the initial low peaks for Xan and UA are caused by contamination of the injectate by the oxidation products (UA and Xa), which appear coincident with the albumin peak because of their low membrane *PS* (33). These curves demonstrate the paucity of break-down products of Hx, as would be expected in an organ lacking Xa dehydrogenase/oxidase.

Ado outflow dilution data: guinea pigs

The normalized outflow dilution curve for one experiment in a guinea pig heart is shown in Fig. 3, *right*. The entire Ado curve is well below that of AraH, again indicating significant cellular uptake and almost no return flux of the injected tracer Ado. The estimated PS_C for Ado (4.31 ± 1.1 ml · g^{-1} · min^{-1}) was almost twice that of AraH (2.39 ± 0.51 ml · g^{-1} · min^{-1}), suggesting that the PS_{ecl} was near 1.9 ml · g^{-1} · min^{-1}. Ado recovery was 38 ± 4%; the conversion to metabolites included Ino (2%), Hx and Xa (combined, 1–2%), and UA (1–11%) detected in the outflow. The UA recovery was certainly incomplete, judging from the form of its outflow dilution curve in Fig. 3. The retained fraction, just under 50%, is presumably mainly in nucleotides.

Examination of the time course of the recovery of these metabolites (Fig. 3, *bottom right*) indicates that conversion of Ado was rapid, with maximum concentrations of the first metabolic product, Ino, occurring almost simultaneously with those of Ado. The peak of [^{14}C]UA, as an end product of tracer Ado metabolism, occurred ~15 s after injection. The forms of the washout curves for UA appear compatible with the endothelial *PS* estimated by Kroll et al. (33). The concentration of Hx is strikingly lower than in the rabbit data. Even though there is a large UA efflux, the concentration of its precursor Xa is very low, indicating either that its cell membrane permeability is very low or that it is not dissociated from the enzyme before it is reacted to produce UA.

We summarize the metabolic data as follows. In the guinea pig heart, 10–15% of Ado was metabolized to wash out into the effluent as Ino (2%), Hx (1%), Xa (1%), or UA (10%); 41% washed out unchanged and ~50% was retained, presumably as nucleotide or oligomeric ATP. Of the injected tracer Ino, 51% washed out unchanged, 25% was metabolized (2% to Hx, 1% to Xa, and ~20% to UA), and 25% was retained. In the rabbit heart, 45% of Ado was retained, ~5% was metabolized to Ino and Hx, and none was metabolized to Xa and UA. For inosine, 90% appeared unchanged in the outflow, ~3% metabolized to Hx, and ~7% was retained. Rabbit hearts lack xanthine oxidase and do not degrade Hx to UA, but the

guinea pig endothelium exhibits higher rates of transport and intracellular reaction for both Ado and Ino.

Model transport parameters

Results of model fitting to the outflow dilution curves are exemplified for rabbit and guinea pig hearts in Figs. 2 and 3. The parameter values for all hearts are summarized in Table 4.

The values for PS_g and PS_{ecl} are estimated more accurately via the modeling analysis than via the Crone-Renkin expression (PS_c) because the back-diffusion is accounted for by fitting the entire curve, including the tail, with the four-region blood-tissue exchange model. The difference between PS_c and the sum of $PS_g + PS_{ecl}$ was smaller for Ado than for Ino, particularly in the guinea pig, because its cellular uptake is higher and its back-diffusion smaller: uptake and retention by endothelial and parenchymal cells in the guinea pig prevented almost all of the reflux from the ISF to plasma, and the observed E(t) remained high throughout the data acquisition period. (The figures show that the Ado curves remain below the albumin curves for the whole 80 s, indicating continued extraction.)

Because the volume of endothelial cells is so small, ~0.02 ml/g, solute entry alone does not produce a fit to the data curves, which requires also endothelial cell metabolism and retention of Ado (G_{ec}). Adjusting values of the parameters describing parenchymal cell transport (PS_{pc}) and metabolism (G_{pc}) does not affect the early portions of the model curves; these parameters are determined from the later portions of the curves. Values are reported in Table 4: the estimates for the parenchymal cells in general are similar to those for endothelial cells for Ado and Ino.

DISCUSSION

These experiments provide evidence that qualitative and quantitative differences exist in endothelial nucleoside transport and metabolism between rabbit and guinea pig hearts. In both rabbit and guinea pig hearts, the early extractions of Ado and Ino are higher than that of a structural analog, AraH, that is not transported by the membrane nucleoside carrier. The greater extraction of these nucleosides relative to AraH can only be explained by permeation of the endothelial luminal plasma membrane. In rabbit hearts, the luminal endothelial uptake of these nucleosides is small. Uptake of Ado and Ino by myocytes or through the abluminal endothelial surface can occur after the substances reach the ISF, which reduces their back-diffusion from ISF to plasma compared with that for AraH. However, such back-diffusion has no significant influence on the apparent extractions during the up-slope to the peak of the dilution curves, because the ISF concentration is still close to zero in the first few seconds.

This qualitative analysis is supported by the quantitative analysis using a model that accounts for endothelial cell uptake and metabolism of Ado and Ino. This model makes use of the whole curves, rather than just early extraction, to estimate separately the contributions of paracellular diffusional exchange through the interendothelial clefts and endothelial cellular uptake. The guinea pig endothelial cell's greater capacity for nucleoside transport compared with that of rabbit endothelial cells reflects a quantitative rather than a qualitative difference between the species but is most striking. In contrast, neither the rates of myocyte transport nor those of the intracellular reactions appear to differ from those of endothelial cells.

In the analysis, we used the fact that these are tracer experiments with high-specific-activity radioactive compounds so that the chemical, nontracer concentration (C) of Ino or Ado is presumably much lower than the Michaelis-Menten constant (K_m) for the binding sites on

the transporters or enzymes. When this is true, the equations are linear because changing the tracer concentration has no influence on the binding process. The effective *PS* via the transporter when there is competing substrate is $PS_{ecl}(C) = V_{max}S/(K_m + C)$, identifying the PS as being concentration dependent, but when C = 0, then it is maximal and $PS_{max} = PS_{ecl}(C = 0)$ is equivalent to $V_{max}S/K_m$, where V_{max} is a maximal flux (mmol per cm^2 surface area per min) and S is surface area (cm^2/g). Our tracer experiments cannot parse this expression to distinguish V_{max} from K_m, and further experiments are needed to identify the transporter kinetics to a deeper level.

A comment on AraH as an extracellular reference tracer is required. In the presence of dipyridamole, a blocker of the Ado/Ino transporter, Bassingthwaighte and Sparks (5) noted that there was no difference between the outflow curves for Ado and AraH. Measures of AraH recovery by Gorman et al. (26) demonstrated high recovery. Our studies indicate that in the absence of dipyridamole there is an enlarged interstitial volume of distribution for AraH. This might be explained by a transient attachment to binding sites, such as transporter sites (although it is not transported) or Ado receptor sites (although it does not activate vasodilator receptors). Given such events occurring in the interstitium, one might suspect as a corollary that there might be some transient attachment to sites on the endothelial luminal surface; if so, then our estimates of PS_{ecl} would be slightly erroneously low. We cannot repeat these experiments because of the difficulty in obtaining the precursor for AraH, but the way to examine this question would be to make comparisons of estimates of PS_{ecl} for sucrose and AraH in the presence and absence of dipyridamole. However, the potential for such a bias has no influence on the conclusions regarding the differences between Ino and Ado or between the species.

Although this model of capillary transport fits well the rising and peak portions of the outflow curves, the tails of the nucleoside curves are less well fitted. The model curves tend to be above the actual data points over the times from 60 to 100 s. This may be because the model as presently constructed does not adequately describe the heterogeneity present in isolated, perfused hearts. For example, we assume that although flow is heterogeneous, all capillaries have the same PS_g and PS_{ecl}; although PS_g is fairly likely to be more uniform simply because capillary densities are known not to have much variation, transporter densities, and thus PS_{ecl}, may possibly vary regionally with flow. This has been observed for fatty acid by Caldwell et al. (12). The small errors in fitting the tails of the nucleoside curves do not influence our conclusions about species differences in endothelial cell uptake, which are based on earlier portions of the curve where the fitting was quite good.

An assumption made for the purposes of the analysis was that the abluminal endothelial transporter capacity and turnover were similar to those of the endothelial luminal surface, i.e., $PS_{eca} = PS_{ecl}$. This assumption was made because the curve fitting is not very sensitive to different values of PS_{eca} even though there is high sensitivity to PS_{ecl}; the reason is the combination of the high intraendothelial consumption and the fact that uptake from the ISF can be into both parenchymal cells and endothelial cells simultaneously. Gorman et al. (26) had thought that PS_{eca} might be as much as 10-fold greater than PS_{ecl} in canine skeletal muscle, but Wangler et al. (51), studying guinea pig hearts, could not distinguish the effects of PS_{eca} from those of PS_{pc} and therefore estimated only their sum. When they optimized the model fits to their data, they found that an assumption of $PS_{eca} = PS_{ecl}$ and an assumption of $PS_{eca} = 10 \times PS_{pc}$ gave equally good fits, thus affirming the relative insensitivity to the effects of myocyte versus endothelial uptake from the interstitium. Mohrman and Heller (39) estimated PS_{eca}/PS_{ecl} to be ~1.4, judging from nontracer studies of inflow-outflow concentrations in guinea pigs. In affirmation of the lower estimate of the ratio, Dr. Keith Kroll and colleagues (in unpublished guinea pig studies done in our laboratory at the University of Washington) estimated a ratio of 1.0. In their experiments,

they blocked both Ado kinase and Ado deaminase, effectively reducing G_{ec} to zero and greatly increasing the sensitivity of the model fitting to the estimates of PS_{eca}. However, this issue should not be regarded as settled.

Several studies have suggested variability in the number of nucleoside transport sites among species. Species variability in the binding of 8-(*p*-nitrobenzyl)-6-thioinosine (NBTI or NBMPR), a potent and selective inhibitor of nucleoside transport, has been demonstrated in erythrocytes (13,31,32) and in cardiac membrane preparations by Williams et al. (52). In the study by Williams et al., the maximal binding capacity for guinea pig ventricle was more than threefold greater than for rabbit ventricle. A subsequent study by this group (42), which correlated the distribution of NBMPR binding sites with those for von Willebrand factor, an endothelial cell marker, demonstrated in guinea pigs that the majority of the NBMPR binding sites in the membrane preparation can be attributed to endothelial membranes mixed in with the cardiomyocyte membranes.

Species differences in nucleoside transporter would account for differences seen in endothelial cell accumulation of tracer Ado. Guinea pig studies show preferential uptake into endothelial cells (16,40). Rabbit studies show little uptake by endothelial cells (53).

The second, and probably most important, difference between rabbits and guinea pigs is the difference in nucleoside degradation in the two species. These studies suggest that guinea pig endothelial cells, like human erythrocytes (44,45), are fully equipped for uptake and degradation of Ado, the last stages being via Xa oxidase to UA, the most prominent metabolic end product. In contrast, rabbit endothelial cells have poorer transport capacity and apparently lack Xa oxidase; thus Hx is the metabolic end point measured in this species. These data are in agreement with Downey et al. (18,19), who were unable to detect Xa oxidase in rabbit myocardium, and Grum et al. (27), who reported that ischemic rabbit hearts did not produce urate, just as we observed here in normoxic hearts. Differences in expression may be as important as differences in the genes: even the same cell type behaves differently in different locations: Moffett et al. (38) found avid endothelial uptake of serotonin in rabbit lungs but not in heart.

These differences in endothelial nucleoside transport and metabolism are undoubtedly reflected in other differences in purine metabolism among species. As examples of this, Borgers and Thone (10) found in histochemical studies that the locations of 5′-nucleotidase (hydrolyzes AMP to Ado) and purine nucleoside phosphorylase (Ino → Hx) were not generally found in myocytes, with the exception that 5′-nucleotidase is found in rat myocytes but not in human, dog, rabbit, or guinea pig myocytes. The nucleotidase is dominantly extracellular, on the surface of pericytes, and on only endothelial cells of arterioles. Borgers and Thone (10) give references to other aspects of purine metabolism where species differences have been noted in the biochemistry.

Our overall conclusion is that care must be taken when generalizing about nucleoside transport as well as metabolism. Differences between species and between cell types within a species must be considered when evaluating the role of such agents as mediators in pathophysiological processes of coronary artery vasomotion and myocardial ischemia.

APPENDIX

Interstitial Binding of AraH

The binding of a solute to a receptor augments the effective volume of distribution V_d' so that it is larger than its aqueous dilution space (V_d), so $V_d'=V_d - V_B$, where V_B is the

apparent excess space, a virtual binding space. If binding and unbinding are instantaneous, so that there is an equilibrium, then $V_B = V_d \cdot B_T/(K_d + C)$, where B_T is the concentration of the binding sites (molar, equivalent to millimole of specific binding molecule per milliliter of space), K_d is the equilibrium dissociation constant (molar), and C is the solute concentration (molar). The effective volume is then as previously shown by Safford and Bassingthwaighte (46)

$$V_d^{'}=V_d[1+B_T/(K_d+C)].$$

For tracer-only experiments C is zero, so $V_d^{'}=V_d(1+B_T/K_d)$.

Under these conditions we could have used the linear 1989 model (6) simply by allowing $V_{isf}^{'}$ to be a freely adjusted parameter for AraH, but we did not dare to assume that AraH was in equilibrium with the unidentified binding site and instead allowed the binding reactions to be slow. The relevant differential equations augmented the 1989 model so that the interstitial equations were

$$\frac{dCB}{dt}=k_1 \cdot C_{isf}(B_T - CB) - k_1 K_d \cdot CB \quad (A1)$$

$$\frac{dC_{isf}}{dt}= - k_1 C_{isf}(B_T - CB)+k_1 K_d \cdot CB+\frac{PS_g}{V_{isf}^{'}}(C_p - C_{isf}) \quad (A2)$$

where $B_T = CB - B$, the sum of the free (B) and complexed (CB) binding molecule. These are included in a generalized nonlinear model for convection, diffusion, exchange, and transformation, GENTEX, written by Dr. Zheng Li.

Acknowledgments

The modeling and analysis technology was supported by the National Simulation Resource for Circulatory Mass Transport and Exchange, National Center for Research Resources Grant RR-1243. The experimental work and analysis were supported by National Heart, Lung, and Blood Institute Grant HL-19139.

REFERENCES

1. Bardenheuer H, Whelton B, Sparks HV Jr. Adenosine release by the isolated guinea pig heart in response to isoproterenol, acetylcholine, and acidosis: the minimal role of vascular endothelium. Circ. Res. 1987; 61:594–600. [PubMed: 3652402]
2. Bassingthwaighte JB, Chan IS, Wang CY. Computationally efficient algorithms for capillary convection-permeation-diffusion models for blood-tissue exchange. Ann. Biomed. Eng. 1992; 20:687–725. [PubMed: 1449234]
3. Bassingthwaighte, JB.; Goresky, CA. Handbook of Physiology. The Cardiovascular System. The Microcirculation. Bethesda, MD: Am. Physiol. Soc.; 1984. Modeling in the analysis of solute and water exchange in the microvasculature; p. 549-626.sect. 2, vol. IV, pt. 1, chapt. 13
4. Bassingthwaighte JB, Malone MA, Moffett TC, King RB, Little SE, Link JM, Krohn KA. Validity of microsphere depositions for regional myocardial flows. Am. J. Physiol. 1987; 253:H184–H193. (Heart Circ. Physiol. 22). [PubMed: 3605365]
5. Bassingthwaighte JB, Sparks HV. Indicator dilution estimation of capillary endothelial transport. Annu. Rev. Physiol. 1986; 48:321–334. [PubMed: 3518617]
6. Bassingthwaighte JB, Wang CY, Chan IS. Blood tissue exchange via transport and transformation by endothelial cells. Circ. Res. 1989; 65:997–1020. [PubMed: 2791233]

7. Bassingthwaighte JB, Yipintsoi T, Harvey RB. Microvasculature of the dog left ventricular myocardium. Microvasc. Res. 1974; 7:229–249. [PubMed: 4596001]
8. Becker, BF.; Gerlach, E. Uric acid, the major catabolite of cardiac adenine nucleotides and adenosine, originates in the coronary endothelium. In: Gerlach, E.; Becker, BF., editors. Topics and Perspectives in Adenosine Research. Berlin: Springer; 1987. p. 209-222.
9. Berne RM, Knabb RM, Ely SW, Rubio R. Adenosine in the local regulation of blood flow: a brief overview. Federation Proc. 1983; 42:3136–3142. [PubMed: 6641949]
10. Borgers M, Thone F. Species differences in adenosine metabolic sites in the heart. Histochem. J. 1992; 24:445–452. [PubMed: 1506236]
11. Bukowski T, Moffett TC, Revkin JH, Ploger JD, Bassingthwaighte JB. Triple-label β liquid scintillation counting. Anal. Biochem. 1992; 204:171–180. [PubMed: 1514684]
12. Caldwell JH, Martin GV, Raymond GM, Bassingthwaighte JB. Regional myocardial flow and capillary permeability-surface area products are nearly proportional. Am. J. Physiol. 1994; 267:H654–H666. (*Heart Circ. Physiol.* 36). [PubMed: 8067421]
13. Cass CE, Paterson ARP. Inhibition by nitrobenzylthioinosine of uptake of adenosine, 2′-deoxyadenosine and 9-β-d-arabinofuranosyladenine by human and mouse erythrocytes. Biochem. Pharmacol. 1975; 24:1989–1993. [PubMed: 1082336]
14. Catravas JD. Removal of adenosine from the rabbit pulmonary circulation, in vivo and in vitro. Circ. Res. 1984; 54:603–611. [PubMed: 6723004]
15. Chan IS, Goldstein AA, Bassingthwaighte JB. SENSOP: a derivative-free solver for non-linear least squares with sensitivity scaling. Ann. Biomed. Eng. 1993; 21:621–631. [PubMed: 8116914]
16. Deussen A, Moser G, Schrader J. Contribution of coronary endothelial cells to cardiac adenosine production. Pflügers Arch. 1986; 406:608–614.
17. Dieterle Y, Ody C, Ehrensberger A, Stalder H, Junod AF. Metabolism and uptake of adenosine triphosphate and adenosine by porcine aortic and pulmonary endothelial cells and fibroblasts in culture. Circ. Res. 1978; 42:869–876. [PubMed: 657449]
18. Downey JM, Hearse DJ, Yellon DM. The role of xanthine oxidase during myocardial ischemia in several species including man. J. Mol. Cell. Cardiol. 1988; 20:55–63. [PubMed: 3045330]
19. Downey JM, Miura T, Eddy LJ, Chambers DE, Mellert T, Hearse DJ, Yellon DM. Xanthine oxidase is not a source of free radicals in the ischemic rabbit heart. J. Mol. Cell. Cardiol. 1987; 19:1053–1060. [PubMed: 3481402]
20. Edward JT. Molecular volumes and the Stokes-Einstein equation. J. Chem. Ed. 1970; 47:261–270.
21. Ely SW, Berne RM. Protective effects of adenosine in myocardial ischemia. Circulation. 1992; 85:893–904. [PubMed: 1537125]
22. Feigl EO. Coronary physiology. Physiol. Rev. 1983; 63:1–205. [PubMed: 6296890]
23. Gao ZP, Downey HF, Fan WL, Mallet RT. Does interstitial adenosine mediate acute hibernation of guinea pig myocardium? Cardiovasc. Res. 1995; 29:796–804. [PubMed: 7656283]
24. Gerlach E, Nees S, Becker BF. The vascular endothelium: a survey of some newly evolving biochemical and physiological features. Basic Res. Cardiol. 1985; 80:459–474. [PubMed: 3935101]
25. Gonzalez F, Bassingthwaighte JB. Heterogeneities in regional volumes of distribution and flows in the rabbit heart. Am. J. Physiol. 1990; 258:H1012–H1024. (*Heart Circ. Physiol.* 27). [PubMed: 2109937]
26. Gorman MW, Bassingthwaighte JB, Olsson RA, Sparks HV. Endothelial cell uptake of adenosine in canine skeletal muscle. Am. J. Physiol. 1986; 250:H482–H489. (*Heart Circ. Physiol.* 19). [PubMed: 3513628]
27. Grum CM, Ketai LH, Myers CL, Shlafer M. Purine efflux after cardiac ischemia: relevance to allopurinol cardioprotection. Am. J. Physiol. 1987; 252:H368–H373. (*Heart Circ. Physiol.* 21). [PubMed: 3812751]
28. Harmsen E, deJong JW, Seriuys PW. Hypoxanthine production by ischemic heart demonstrated by pressure liquid chromatography of blood purine nucleosides and oxypurines. Clin. Chim. Acta. 1981; 115:73–84. [PubMed: 7261408]

29. Hellewell PG, Pearson JD. Different uptake profiles for prostaglandin Fd2au and adenosine in the piglet pulmonary circulation (Abstract). J. Physiol. (Lond.). 1983; 334:102P.
30. Hopkins SV, Goldie RG. A species difference in the uptake of adenosine by heart. Biochem. Pharmacol. 1971; 20:3359–3365. [PubMed: 5132882]
31. Jarvis SM, Hammond JR, Paterson ARP, Clanachan AS. Species differences in nucleoside transport: a study of uridine transport and nitrobenzylthioinosine binding by mammalian erythrocytes. Biochem. J. 1982; 208:83–88. [PubMed: 7159400]
32. Jarvis SM, Young JD. Nucleoside translocation in sheep reticulocytes and fetal erythrocytes: a proposed model for the nucleoside transporter. J. Physiol. (Lond.). 1982; 324:47–66. [PubMed: 6284922]
33. Kroll K, Bukowski TR, Schwartz LM, Knoepfler D, Bassingthwaighte JB. Capillary endothelial transport of uric acid in the guinea pig heart. Am. J. Physiol. 1992; 262:H420–H431. (*Heart Circ. Physiol.* 31). [PubMed: 1539702]
34. Kroll K, King RB, Caldwell JC, Krohn KA, Rhodes CA, Bassingthwaighte JB. Distributed non-linear modeling of PET adrenoreceptor ligand. Ann. Biomed. Eng. 1995; 23 S-64.
35. Kroll K, Stepp DW. Adenosine kinetics in the canine coronary circulation. Am. J. Physiol. 1996; 270:H1469–H1483. (*Heart Circ. Physiol.* 39). [PubMed: 8967391]
36. Kuikka J, Levin M, Bassingthwaighte JB. Multiple tracer dilution estimates of D- and 2-deoxy-D-glucose uptake by the heart. Am. J. Physiol. 1986; 250:H29–H42. (*Heart Circ. Physiol.* 19). [PubMed: 3510568]
37. McConahey PJ, Dixon FJ. A method of trace iodination of proteins for immunologic studies. Int. Arch. Allergy. 1966; 29:185–189. [PubMed: 4160044]
38. Moffett TC, Chan IS, Bassingthwaighte JB. Myocardial serotonin exchange: negligible uptake by capillary endothelium. Am. J. Physiol. 1988; 254:H570–H577. (*Heart Circ. Physiol.* 23). [PubMed: 3279823]
39. Mohrman DE, Heller LJ. Transcapillary adenosine transport in isolated guinea pig and rat hearts. Am. J. Physiol. 1990; 259:H772–H783. (*Heart Circ. Physiol.* 28). [PubMed: 2396688]
40. Nees S, Herzog V, Becker BF, Böck M, Des Rosiers C, Gerlach E. The coronary endothelium: a highly active metabolic barrier for adenosine. Basic Res. Cardiol. 1985; 80:515–529. [PubMed: 3000345]
41. Olsson RA, Khouri EM, Bedynek JL Jr, McLean J. Coronary vasoactivity of adenosine by pig aortic endothelial and smooth muscle cells in culture. Circ. Res. 1979; 45:468–478. [PubMed: 476869]
42. Parkinson FE, Clanachan AS. Heterogeneity of nucleoside transport inhibitory sites in heart: a quantitative autoradiographical analysis. Br. J. Pharmacol. 1989; 97:361–370. [PubMed: 2788021]
43. Pearson JD, Carleton JS, Hutchings A, Gordon JL. Uptake and metabolism of adenosine by pig aortic endothelial and smooth-muscle cells in culture. Biochem. J. 1978; 170:265–271. [PubMed: 637842]
44. Plagemann PGW, Wohlhueter RM. Kinetics of nucleoside transport in human erythrocytes alterations during blood preservation. Biochim. Biophys. Acta. 1984; 778:176–184. [PubMed: 6498185]
45. Plagemann PGW, Wohlhueter RM, Erbe J. Nucleoside transport in human erythrocytes: a simple carrier with directional symmetry and differential mobility of loaded and empty carrier. J. Biol. Chem. 1982; 257:12069–12074. [PubMed: 7118930]
46. Safford RE, Bassingthwaighte JB. Calcium diffusion in transient and steady states in muscle. Biophys. J. 1977; 20:113–136. [PubMed: 901900]
47. Schrader, J. Sites of action and production of adenosine in the heart. In: Burnstock, G., editor. Purinergic Receptors. Vol. vol. 12. London: Chapman and Hall; 1981. p. 121-162.(*Receptors and Recognition*, Ser. B)
48. Stepp DW, van Bibber R, Kroll K, Feigl EO. Quantitative relation between interstitial adenosine concentration and coronary blood flow. Circ. Res. 1996; 79:601–610. [PubMed: 8781493]
49. Vargas FF, Johnson JA. An estimate of reflection coefficients for rabbit heart capillaries. J. Gen. Physiol. 1964; 47:667–677. [PubMed: 14127605]

50. Vargas FF, Johnson JA. Permeability of rabbit heart capillaries to non-electrolytes. Am. J. Physiol. 1967; 213:87–93. [PubMed: 6027941]

51. Wangler RD, Gorman MW, Wang CY, DeWitt DF, Chan IS, Bassingthwaighte JB, Sparks HV. Transcapillary adenosine transport and interstitial adenosine concentration in guinea pig hearts. Am. J. Physiol. 1989; 257:H89–H106. (*Heart Circ. Physiol.* 26). [PubMed: 2750952]

52. Williams EF, Barker PH, Clanachan AS. Nucleoside transport in heart: species differences in nitrobenzylthioinosine binding, adenosine accumulation and drug-induced potentiation of adenosine action. Can. J. Physiol. Pharmacol. 1984; 62:31–37. [PubMed: 6713281]

53. Winkler B, Seiler R, Schaper W. Single passage of adenosine in the rabbit heart at low and high adenosine concentrations (Abstract). FASEB J. 1988; 2:A1883.

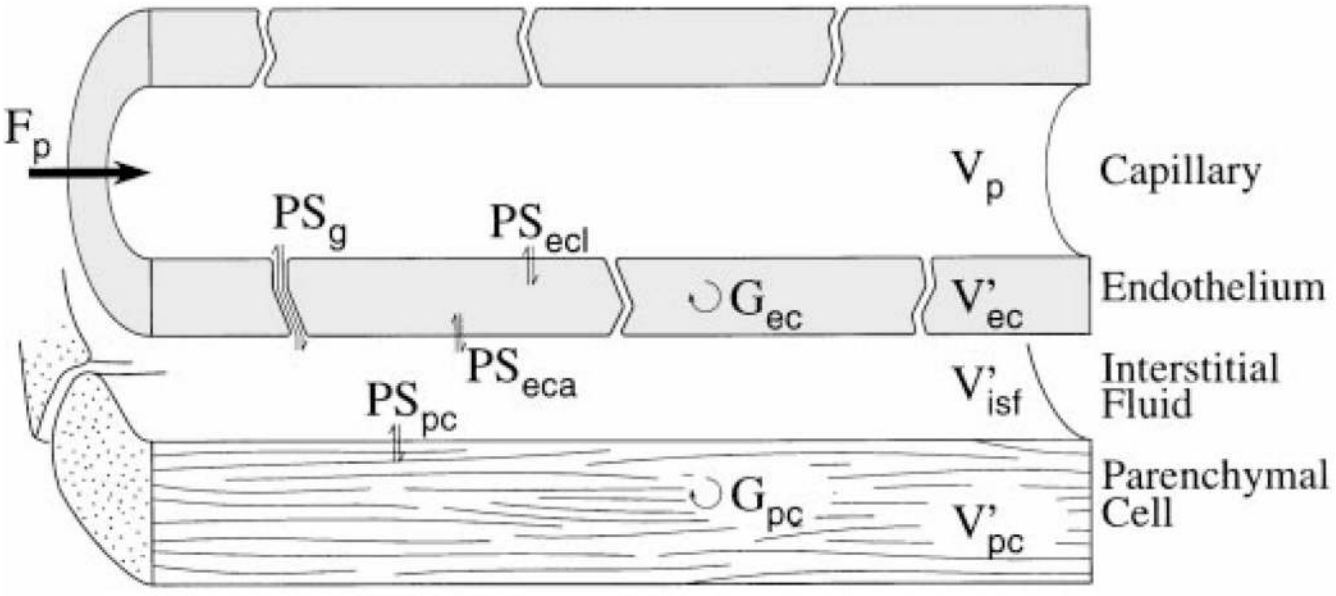

Fig. 1.

Schematic of 4-region, 3-barrier model for blood-tissue exchange used for analysis of indicator dilution curves. Parameter symbols are defined in *Glossary*. The analysis used a set of such modules in parallel to account for flow heterogeneity.

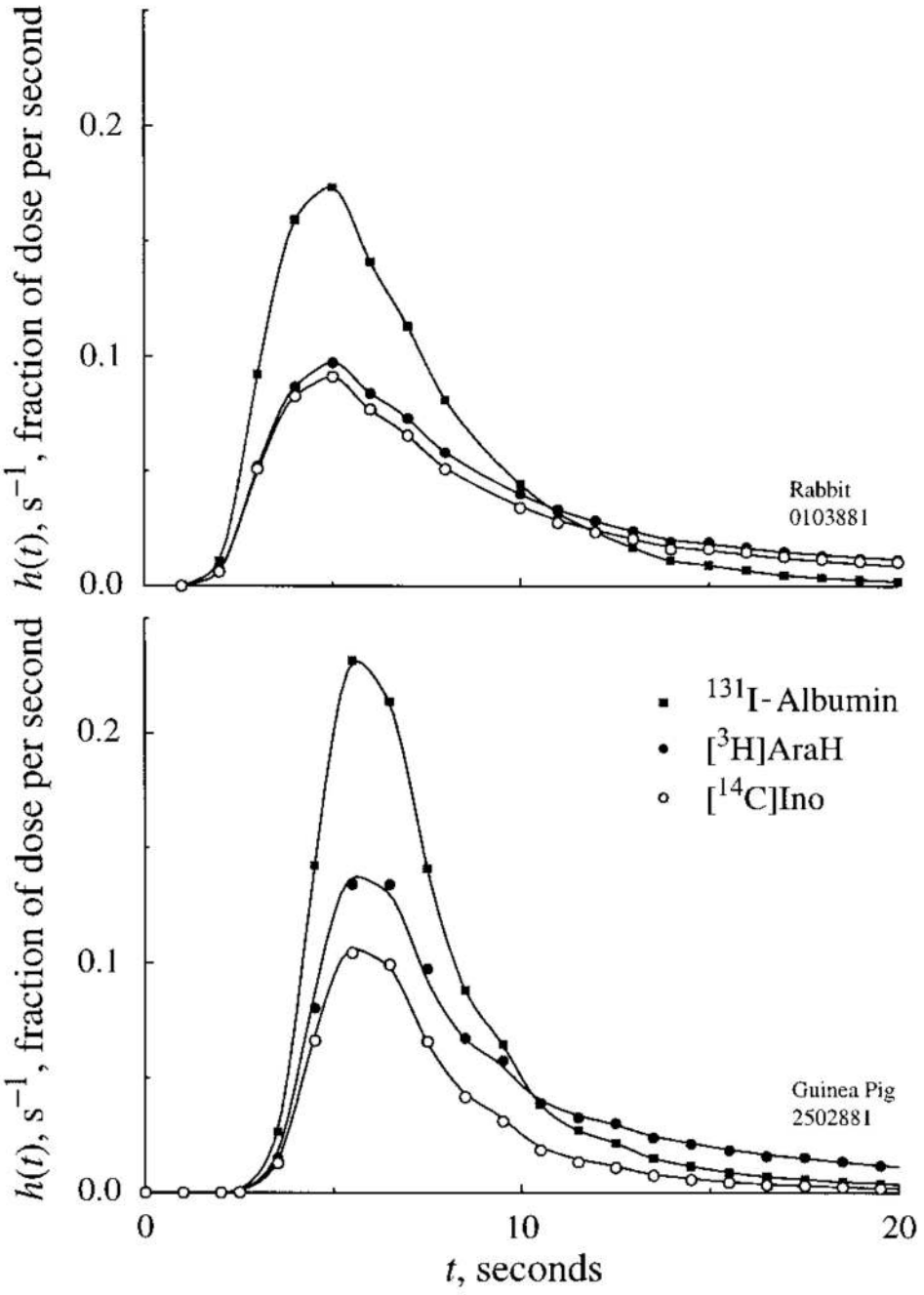

Fig. 2.

Coronary sinus outflow dilution curves for [^{14}C]inosine ([^{14}C]Ino), [^{3}H]arabinofuranosyl hypoxanthine ([^{3}H]AraH), and ^{131}I-albumin; model solutions are continuous lines. Extractions and recoveries are listed in Tables 1 and 2. Parameters for model fits are in Table 4; each estimate is given with its individual standard deviation. *Top*: data from an isolated, perfused rabbit heart. $F_p = 3.89$ ml · g^{-1} · min^{-1}. *Bottom*: data from an isolated, perfused guinea pig heart. $F_p = 3.57$ ml · g^{-1} · min^{-1}. Note that Ino curve is lower than AraH curve, indicating higher values of PS_{ecl} in guinea pig compared with rabbit.

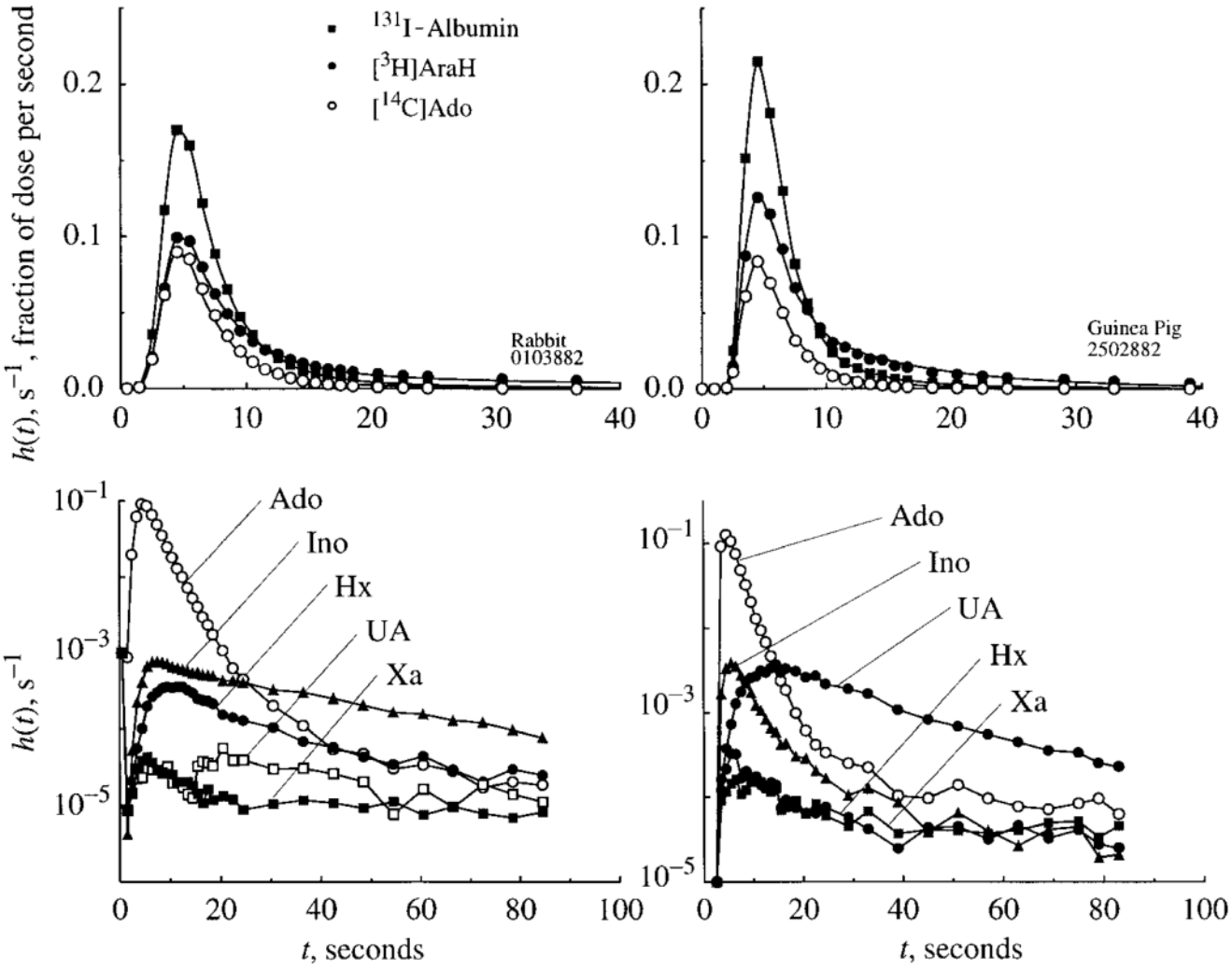

Fig. 3.

Adenosine (Ado) transport and transformation in isolated, perfused rabbit (*left*) and guinea pig (*right*) heart. *Top panels*: normalized outflow dilution curves for [^{14}C]Ado and the 2 reference tracers, ^{131}I-albumin (intravascular) and [^{3}H]AraH (extracellular); model solutions are shown by lines. *Bottom panels*: semilog plot of Ado and its metabolites, Ino, hypoxanthine (Hx), xanthine (Xa), and uric acid (UA), in the outflow. The Ado curve is the same as in panel above. Linesjoin data points and are not model solutions. Note striking difference in shapes of effluent curves for metabolites in the 2 species. Curves labeled UA and Xa from the rabbit (*bottom left*) are not quantifiable, isotope count rates being 10^{-5} times those of albumin curve.

Table 1

Data summary

Expt. No.	Nucleoside Injected	F_p, ml · g^{-1} · min^{-1}	E_{max}, %			PS_c, ml · g^{-1} · min^{-1}			% Recovery of Injectate (Ado or Ino)
			AraH	Ino	Ado	AraH	Ino	Ado	
				Rabbit					
0103881	Ino	3.89	45	48		2.33	2.54		91
2502884	Ino	4.94	47	52		3.14	3.63		85
2010871	Ino	4.43	58	57		3.84	3.74		94
2010872	Ino	4.38	56	56		3.60	3.60		86
Mean ± SD (n = 4)							3.38 ± 0.56		89 ± 4
0103882	Ado	3.83	43		47	2.15		2.43	50
2502885	Ado	5.17	46		50	3.19		3.58	53
2010873	Ado	4.41	52		54	3.24		3.42	51
2010874	Ado	4.49	50		51	3.11		3.20	57
Mean ± SD (n = 4)								3.16 ± 0.57	53 ± 3
Mean ± SD (n = 8)		4.4 ± 0.4	50 ± 5	53 ± 4	51 ± 2	3.08 ± 0.58			
				Guinea pig					
0103884	Ino	6.41	37	52		2.96	4.70		51
2502881	Ino	3.57	44	55		2.07	2.85		47
2409871	Ino	4.87	32	56		1.88	4.00		50
2409872	Ino	4.67	37	50		2.16	3.24		54
Mean ± SD (n = 4)							3.70 ± 0.82		51 ± 3
0103884	Ado	6.65	39		59	3.29		5.93	39
2502882	Ado	3.76	42		61	2.05		3.54	37
2409873	Ado	4.97	41		56	2.62		4.08	39
2409874	Ado	5.18	33		51	2.07		3.70	50
Mean ± SD (n = 4)								4.31 ± 1.1	41 ± 5
Mean ± SD (n = 8)		5.0 ± 1.0	38 ± 4	53 ± 2	57 ± 4	2.39 ± 0.51			

F_p, flow of solute-containing perfusate; E_{max}, maximal instantaneous extraction; AraH, 9-β-D-arabinofuranosyl hypoxanthine; Ino, inosine; Ado, adenosine; PS_c, capillary permeability-surface area product calculated via Eq. 1; n, no. of experiments.

Table 2

Metabolites in effluent

Expt. No.	Injectate	Fraction of Injectate Appearing as					Injectate Total
		Ado	Ino	Hx	Xa	UA	
			Rabbit				
0103881	Ino		91	3	0	1	94
2502884	Ino		85	5	1	1	92
2010871	Ino		94				
2010872	Ino		86				
Mean ± SD			89 ± 4				
0103882	Ado	50	3	1	0	0	54
2502885	Ado	53	3	1	0	0	57
2010873	Ado	51					
2010874	Ado	57	5	1	0	0	63
Mean ± SD		53 ± 3					
			Guinea pig				
0103884	Ino		51	1	1	20	73
2502881	Ino		47	2	1	23	73
2409871	Ino		50				
2409872	Ino		54	2	1	18	75
Mean ± SD			50 ± 3				
0103885	Ado	39	1	1	0	8	49
2502882	Ado	37	3	1	1	11	53
2409873	Ado	39					56
2409874	Ado	50	2	0	0	1	53
Mean ± SD		41 ± 6					53 ± 3

Hx, hypoxanthine; Xa, xanthine; UA, uric acid. Blank spaces indicate data not determined.

Table 3

Capillary wall conductances

	AraH		Ino			Ado		
	PS_c (E_{max}, F)	PS_g (Model)	PS_c (E_{max}, F)	PS_g(= AraH)	PS_{ecl} (Model)	PS_c (E_{max}, F)	PS_g (= AraH)	PS_{ecl} (Model)
Rabbit								
Mean ± SD	3.08 ± 0.6	3.92 ± 0.88	3.38 ± 0.56	4.27 ± 1.0	0.1 ± 0.2	3.16 ± 0.51	3.58 ± 0.7	0.2 ± 0.1
n	8	8	4	4	4	4	4	4
Guinea pig								
Mean ± SD	2.39 ± 0.51	2.58 ± 0.6	3.70 ± 0.8	2.5 ± 0.5	1.7 ± 0.4	4.3 ± 1.1	2.67 ± 0.7	2.0 ± 0.5
n	8	8	4	4	4	4	4	4

Parameter values (in ml · g $^{-1}$ · min^{-1}) were calculated by methods indicated in parentheses. PS_g, *PS* for gaps between adjacent endothelial cells; PS_{ecl}, *PS* for endothelial cell luminal or plasma surface.

Am J Physiol. Author manuscript; available in PMC 2012 October 29.

Table 4

Ado and Ino transport in rabbit and guinea pig hearts

Expt. No.	Solute	Cleft PS_g (AraH), ml · g^{-1} · min^{-1}	Endothelial Cell PS_{ecl}, ml · g^{-1} · min^{-1}	Endothelial Cell G_{ec}, ml · g^{-1} · min^{-1}	Myocyte PS_{pc}, ml · g^{-1} · min^{-1}	Myocyte G_{pc}, ml · g^{-1} · min^{-1}	CV, % AraH	CV, % Permeant
				Rabbit				
0103881	Ino	2.98	0.1 ± 0.0	2 ± 4	36 ± 7	1.4 ± 0.3	1.1	2.2
2502884	Ino	3.94	0.4 ± 0.1	3 ± 2	36 ± 2	2.5 ± 0.7	2.8	7.2
2010871	Ino	5.18	0.0 ± 0.0	0 ± 0	27 ± 7	3.5 ± 0.6	2.7	8.2
2010872	Ino	4.96	0.0 ± 0.0	0 ± 0	26 ± 5	3.8 ± 0.5	3.1	6.3
Mean ± SD		4.3 ± 1.0	0.1 ± 0.2	1 ± 2	31 ± 6	2.8 ± 1.1		
0103882	Ado	2.57	0.3 ± 0.2	6 ± 5	19 ± 5	20 ± 5	3.2	5.0
2502885	Ado	3.95	0.2 ± 0.1	10 ± 25	29 ± 15	23 ± 10	3.3	3.2
2010873	Ado	4.06	0.1 ± 0.1	1 ± 43	20 ± 7	62 ± 43	4.3	4.7
2010874	Ado	3.75	0.1 ± 0.1	4 ± 23	29 ± 12	15 ± 5	2.7	4.1
Mean ± SD		3.6 ± 0.7	0.2 ± 0.1	5 ± 4	24 ± 6	30 ± 21		
All rabbits		3.92 ± 0.88						
				Guinea pig				
0103884	Ino	3.23	1.9 ± 0.3	27 ± 22	76 ± 24	19 ± 6	4.4	6.2
2502881	Ino	2.30	1.5 ± 0.2	22 ± 5	36 ± 13	22 ± 13	6.9	5.1
2409871	Ino	2.31	2.0 ± 0.4	13 ± 9	99 ± 9	23 ± 9	5.4	16.5
2409872	Ino	2.12	1.3 ± 0.2	2 ± 11	49 ± 11	49 ± 11	6.1	5
Mean±SD		2.5 ± 0.5	1.7 ± 0.4	16 ± 11	65 ± 28	28 ± 14		
0103885	Ado	3.77	2.7 ± 0.2	50 ± 29	77 ± 26	109 ± 29	2.3	8.4
2502882	Ado	2.39	2.0 ± 0.2	14 ± 3	15 ± 3	17 ± 3	6.5	10.3
2409873	Ado	2.36	1.8 ± 1.4	14 ± 178	40 ± 128	56 ± 181	9.5	10.9
2409874	Ado	2.17	1.4 ± 0.2	83 ± 311	224 ± 310	245 ± 309	4.4	8.4
Mean±SD		2.7 ± 0.7	2.0 ± 0.5	40 ± 33	89 ± 93	107 ± 100		
All guinea pigs		2.58 ± 0.59						

Values taken for PS_g for Ino and Ado are those found for AraH. Each parameter is estimated from the model fit to the data set and reported as mean ± SD of estimate computed from covariance matrix calculated from local sensitivity functions for all free parameters. G_{ec} and G_{pc}, first-order clearance by consumption or gulosity in endothelial cells and parenchymal cells (myocytes), respectively; CV, coefficient of variation.